Proceedings of the Canadian Society for Mechanical Engineering International Congress
32nd Annual Conference of the Computational Fluid Dynamics Society of Canada
Canadian Society of Rheology Symposium
CSME-CFDSC-CSR 2025
May 25–28, 2025, Montréal, Québec, Canada

ANALYSIS OF TEMPERATURE EVOLUTION ALONG SCANNING TRAJECTORY DURING LASER REMELTING

Anirejuoritse A. Coker[1], Evgueni V. Bordatchev[2,1*], O. Remus Tutunea-Fatan[1,2**]
[1]Department of Mechanical and Material Engineering, Western University, London, Canada
[2]Automotive and Surface Transportation, National Research Council of Canada, University 2, London, Canada
*evgueni.bordatchev@nrc-cnrc.gc.ca, **rtutunea@eng.uwo.ca

Abstract—Surface engineering by laser remelting is a niche advanced manufacturing technology that purposely modifies a surface topography without the addition or removal of material. By contrast, redistribution of molten material occurs through laser remelting to take place along a designated laser path trajectory. This study focuses on the analysis of temperature evolution along a scanning trajectory during surface patterning by laser remelting. For this purpose, several laser remelting experiments were performed while recording live and with high speed the temperature as well as the scanning trajectory in the laser-material interaction zone. Two sample patterns - square and octagon - were laser processed with a constant power of 30 W and scanning speeds of 100 mm/s and 300 mm/s. After this, surface topographies were measured to relate surface profile variations to temperature evolution. The preliminary results obtained indicated that the evolution of the temperature distribution predominantly depends on process parameters such as scanning speed, trajectory length, pattern configuration, and laser power. These findings open up new directions in the development of scientific knowledge and engineering solutions geared towards AI-based control and optimization of the laser remelting processes.

Keywords-laser remelting; scanning trajectory; pyrometer; temperature; evolution; analysis

I. INTRODUCTION

The significance and applicability of laser-based technologies in modern manufacturing, particularly in microfabrication, denotes the need for improved efficiency and productivity in a wide range of applications in aerospace, automotive, and biomedical industries [1]. Three major types of laser-based microfabrication technologies exist: additive [2], subtractive [3], and based on material redistribution. Laser additive manufacturing (cladding, direct deposition, sintering, consolidation, fusion, etc.) relies on high intensity continuous-wave or pulsed laser beams to fuse the workpiece material layer by layer in order to create parts with complex geometries. By contrast, laser subtractive manufacturing removes material through laser ablation to instantly heat up, boil and eventually vaporise the material. Some laser ablation processes include direct laser writing, direct laser interference patterning, and laser induced surface structuring. A common challenge for these two processes is their inability to produce parts with a good surface quality. Because of this, any functional parts fabricated through additive and subtractive laser technologies will generally require a secondary surface polishing operation.

The material redistribution approach relies on a laser remelting (LRM) process for manipulation of the material in a molten state over the top surface. In general terms, material redistribution by LRM can be placed somewhere between additive and subtractive processes since no material is added or removed. LRM is a versatile technology since it can be tailored towards three main types of applications namely: surface polishing (SPo), surface structuring (SS), surface texturing (ST), and surface patterning (SPa). Some of the LRM advantages revolve around high-speed, high-precision, and 24/7 CNC-based operation along with the increased surface quality, microhardness, gloss, and corrosion resistance.

SPo-LRM uses a continuous-wave or pulsed laser beam energy to enhance the surface quality of a workpiece. SPo-LRM melts a superficial layer of the surface, redirects molten material along a scanning trajectory, and allows it to rapidly resolidify. This cycle yields a new and smoother surface topography without losing any material, and with an enhanced post-processed surface quality [4-6]. As the laser beam melts one spot, the adjacent material is also affected by the heat and this in turn will cause preheating as the beam moves along its preset trajectory. This is an important phenomenon to consider when analyzing the temperature evolution during any LRM process.

SS-LRM process [7-9] alters the surface topography by reallocating a molten superficial layer of material. SS-LRM requires a synchronous control of laser intensity, speed, and power along laser path trajectory. In addition to the already mentioned advantages of the SP-LRM process and unlike subtractive manufacturing processes like laser ablation – in

This research was funded by the Natural Science Engineering Research Council of Canada under grants RGPIN/6616-2019 and RGPIN/5126-2019.

which material removal is irreversible – SS-LRM process is reversible. this means that existing geometrical microfeatures (microstructure and/or texture) can be modified to new designs as many times as needed, even restoring initial designs and locations through the inverse LRM process [10].

One additional variant exists for the LRM process, namely surface patterning. During SPa-LRM, top surface is also locally remelted and modified in accordance with a pre-programmed functional pattern. SPa-LRM typically produces a surface pattern as a set of linear and curvilinear geometrical features (points, lines, curves, etc.) typically forming bumps [11], riblets [12], or remelted laser tracks and geometric shapes (circles, triangles, squares, etc.) [13] for wear resistance and lubricant retention by a localised modification of the surface roughness. This technology is still in its early developmental stages towards its own unique industrial applications.

Manufacturing industries use surface quality, structures, patterns, and textures as an important requirement to determine material/part performance, appearance, and durability. Ongoing research strives to further enhance the capabilities of LRM technology, by exploring new laser sources, optimizing process parameters, and integrating LRM with other advanced manufacturing techniques, such as additive and subtractive. As manufacturing evolves constantly, the concept of digital twins began to be used in laser-based manufacturing in an attempt to allow accurate simulations and efficiency enhancements prior as well as during the process [14]. The underlying idea in this case is that a digital twin (DT) should mimic the actual functional performance of the process by replicating it digitally.

The main challenge for the industrial usage of all laser-based microfabrication processes consists in its dependence on various factors. These include physical/mechanical properties of the workpiece material, laser processing parameters as related to energy transfer (optics and motion), complex thermodynamics of laser-material interactions as well as other specific details of the process and of the entire opto-electro-mechanical system. In practice, LRM optimization involves the adjustment of key process parameters (scanning speed, laser power, and focus position) to control the stability of melt pool formation. The measurement of melt pool width is particularly important for understanding of the LRM regimes, estimation of the depth of the solidified melt pool, and identification of any process anomalies together with other features of interest.

Numerous efforts have been made to monitor process performance in real-time by means of embedded optical, acoustic, and thermal emission sensors [15]. Within this wide range of sensors, the use of photodiodes and pyrometers is one of most cost-efficient, high-speed, and reliable instruments for online acquisition of the actual temperature in the laser-material interaction zone. For instance, a pyrometer can be used to control the SP-LRM process by continuously measuring the temperature in the molten pool and adjusting the laser power accordingly [16]. Also, a functional prototype involving coaxial single-camera and two-wavelength imaging pyrometry was used to monitor the melt pool of a continuous laser track. The experimental results have demonstrated the capabilities and the applicability of this particular type of pyrometer-based system for accurate large-scale melt pool monitoring in a laser powder bed fusion process. This represents a first step towards the development of DT with downstream effects on cyber-physical models, optimization as well as control strategies.

The primary focus of this study was to perform the analysis of temperature evolution while laser moves along a designated scanning trajectory during a SPa-LRM process used to microfabricate functional patterns. The study will analyze the pre- and post-heating effects that are present during the SPa-LRM process. These effects are dependent on the pre-set of process parameters, such as scanning speed, laser power, and laser trajectory design and dimensions. It is anticipated that if the laser beam of a LPa-LRM process will move at a lower speed and/or on a longer length trajectory while keeping the power constant, the effect of pre-heating the material in the laser-material interaction zone will be more prominent. Therefore, a two-color infrared pyrometer was used to measure the overall temperature along the laser scanning path in an attempt to discover relationships between process parameters, temperature distribution, and surface topography.

II. Investigational Methodology

A. SP-LRM Experimental Setup

The multifunctional system for performing various LRM processes and operations (polishing, structuring, texturing, patterning), presented in Fig. 1, was developed at the National Research Council of Canada (London, ON, Canada) and was used for research purposes. The LRM system integrates several opto-electro-mechanical components as follows: 1) three-axis motion system from AEROTECH, Inc. (Pittsburgh, PA, USA) mounted on a granite table for precisely positioning a workpiece within a work envelope; 2) two-axis laser scanner from SCANLAB GmbH (Puchheim, Germany) with a *f*-theta lens, having a focusing distance of 256 mm; and 3) continuous wave (cw) laser from IPG Photonics, Inc. (Oxford, MA, USA) with a wavelength of 1070 nm and power up to 100 W. During LRM processing, laser beam was delivered through optical fiber into the scanner after collimating.

The process parameters of the laser (power) and of the scanner (scanning speed and trajectory) are controlled by means of a Windows-based software termed LasPC from the Fraunhofer Institute for Laser Technology (Aachen, Germany). The software enables the synchronization between X_s-Y_s scanner positions, laser switching-on/off and varying laser power. The positions X_k-Y_k-Z_k of kinematic stages are commanded by an additional software developed by AEROTECH, Inc. This CNC software was used to ensure the proper positioning of the sample under the scanner as well as for setting an optimal working (focus) distance. The experiments were performed on a workpiece with 50 mm × 50 mm × 10 mm dimensions made from ground H13 tool steel and mounted within an Argon-filled enclosure to prevent oxidation in the laser-material interaction zone.

During the SPa-LRM experiments, three surface patterns – square, octagon, and triangle – were produced with 100 mm/s and 300 mm/s scanning speeds. Nonetheless, for preliminary investigation reasons, only square and octagon patterns will be detailed in this study. The square pattern had a side length of 8 mm, and the octagon was placed inside 4 mm × 4 mm square

area. Since the focus of this study was on the analysis of temperature distribution evolution along the laser path trajectory with different patterns and speeds, experiments were performed at a constant power of 30 W. To ensure accurate and reliable results, a 20-minute time gap was provided before producing each pattern. This lapse was required to ensure repeatable initial temperature conditions of the workpiece. After completing SPa-LRM experiments, the surface topographies of the produced patterns were scanned by means of an optical profilometer WYKO NT1100 (Veeco Ltd., USA) characterized by a vertical resolution of 0.1 nm and an X-Y grid size of 192.98 nm.

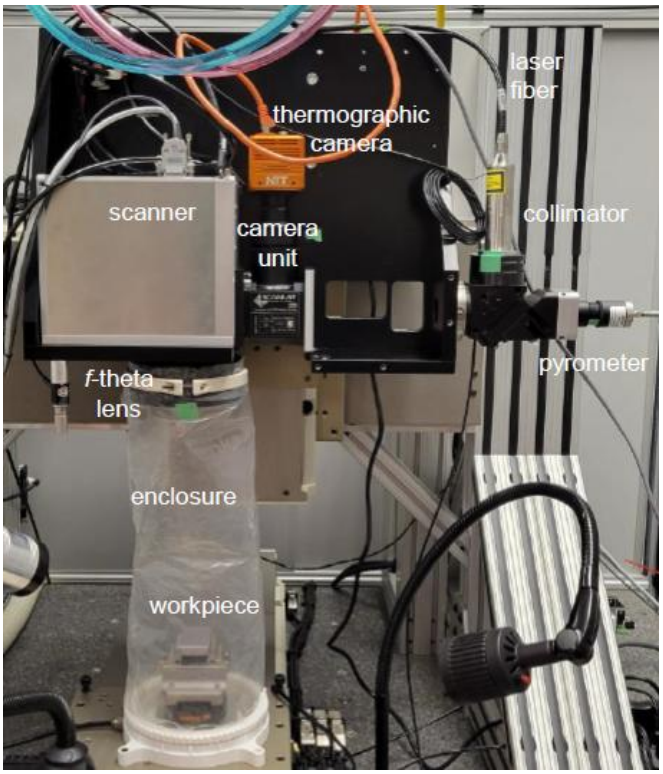

Figure 1. LRM experimental setup.

For measuring the temperature in the laser processing zone, the LRM system was purposely equipped with a two-color infrared (IR) pyrometer (Dr. Mergenthaler GmbH, Germany). The thermographic (TG) IR emission from the laser-material interactions was radiated into the scanner and reflected by its galvanometric mirrors towards the pyrometer. A focusing lens with a focal distance of 50 mm was placed in front of the optical fiber with a core diameter of 50 µm in order to concentrate the IR emission onto the optical fiber (for its further delivery to the pyrometer). This optical setup will capture TG emissions from a circular field-of-view with a diameter of 0.9 mm covering both molten pool and temperature distribution in the surrounding area. It is important to reiterate that pyrometer will measure an average temperature within this field-of-view only by integrating the actual temperature distribution. The control box of the pyrometer works as an analog-digital converter and delivers analog signal within the 0 V to 10 V range that corresponds to a preset temperature range of 163°C to 3000°C. However, the design and settings of the pyrometer do not allow recordings of the average temperature below 163°C.

B. Methodology of Experimental Data Analysis

The analysis of temperature distribution evolution along the laser path trajectory requires high-speed, real time, synchronous data acquisition for four parameters: time, X_s coordinate, Y_s coordinate as well as the analog signal from the pyrometer. This procedure was performed by means of an in-house developed data acquisition software [17] used for recording actual data with a sampling frequency of 100 kHz. This software – to be the prototype of a digital twin of the LRM process – has a dual functionality: i) concurrent execution of a laser processing program and ii) online data recording into computer virtual memory. After completing the laser path trajectory, data are saved offline into a text file to be used for further analysis.

The assessment of the temperature distribution evolution was performed by a user-developed MATLAB function. This function reads the data file encompassing the four recorded parameters and displays two types of plots: i) temperature evolution along X_s-Y_s laser path trajectory and ii) temperature evolution in time domain or along travel distance. Qualitative and quantitative analysis was performed by recognizing distinctive points along the laser path trajectory together with their corresponding locations on the temperature-time plot (turning/bending points at corners). This approach is meant to provide insight on the temperature behaviour at these points as well as between them.

III. Analysis of Temperature Evolution

Fig. 2a depicts surface topography associated with a square pattern produced through SPa-LRM with 100 mm/s speed. For a detailed analysis of the temperature evolution, the surface pattern will be associated with the temperature records in spatial and time domains shown in Fig. 2b and Fig. 2c, respectively. Following this, the following qualitative and quantitative observations can be made:

- Laser trajectory starts with {0, 0} X_s/Y_s coordinates at point A and having laser turned off (laser power equals 0 W). At this point, pyrometer indicates a temperature of 163°C that corresponds to the low cutoff point.
- The laser beam with 0 W power moves to the bottom left corner of the square ({-4, -4} coordinates). This corresponds to point B, where laser power is changed to 30 W. This point corresponds to the start of the remelting along the square pattern.
- From the beginning of line B-C, the remelted pattern continues to form without a changing temperature measurement. This occurs for 38.6 ms from the beginning of the patterning procedure.
- At this moment, temperature starts raising from 163°C to 221°C at the end of line B-C (point C) that corresponds to the 87 ms timestamp.
- The temperature will continue to climb along the vertical line C-D. After the -90° turn will reach 253°C at point D. The laser beam trajectory will make the next -90° turn at point D.
- During the horizontal move along line D-E, the temperature stays stable for a short period of time of ~14 ms until 190 ms timestamp and then starts declining to reach 239°C at point E (top left corner).

- On the last move along the vertical line E-F, the temperature continues to decline to reach 239°C at point F (250 ms timestamp).

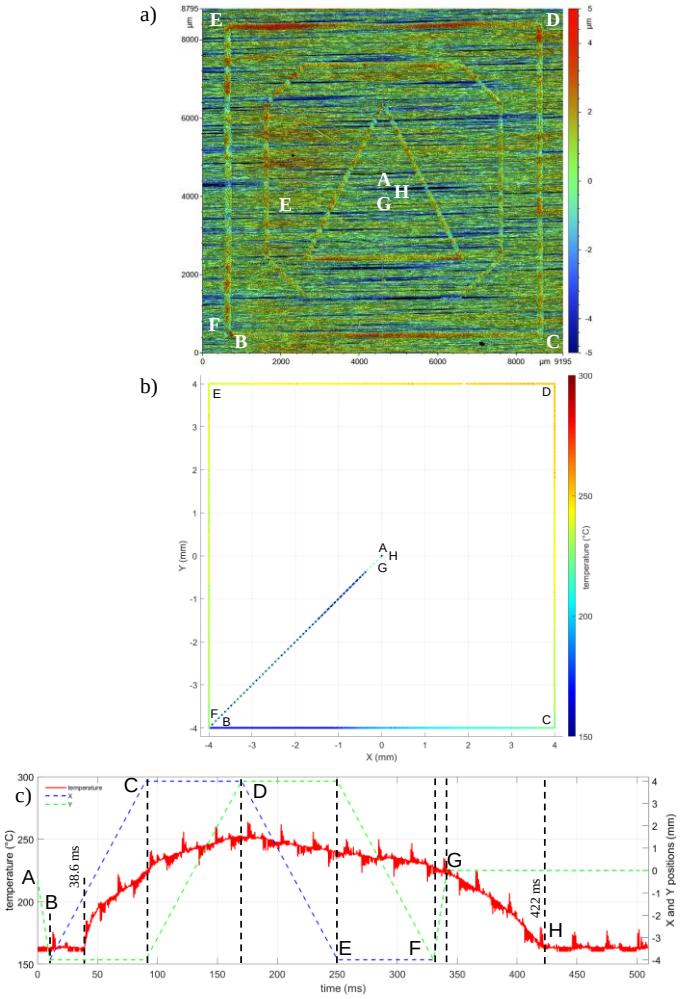

Figure 2. Temperature evolution along the square pattern travelled at 100 mm/s: a) surface topography, b) spatial domain, and c) time domain.

- At this location (F), laser power is set to 0 W and laser beam moves back to the center of the square at point G (identical to point A) and stays at this location. This shows a continuous temperature decline to 163°C (422 ms timestamp) due to thermal conduction and radiation (dissipation, in general).

The described temperature evolution during square patterning at 100 mm/s was compared with a process tracing an identical trajectory but performed at 300 mm/s (Fig. 3a). For a detailed analysis of the temperature evolution similar to the one outlined above, the pattern associated with temperature records in spatial and time domains shown in Fig. 3b and Fig. 3c, respectively. Since laser path trajectories are identical for the same square pattern whereas scanning speed is 3 times faster, the pyrometer starts recording the overall temperature above 163°C only at 72.7 ms timestamp (compared to 38.6 ms at 100 mm/s). Also, the temperature reaches 174°C at point E (compared to 239°C) and exhibits a maximum temperature of 179°C at point F (118 ms timestamp). One other observation is that temperature decreases to 163°C the 129 ms timestamp (versus 422 ms) right after reaching point H.

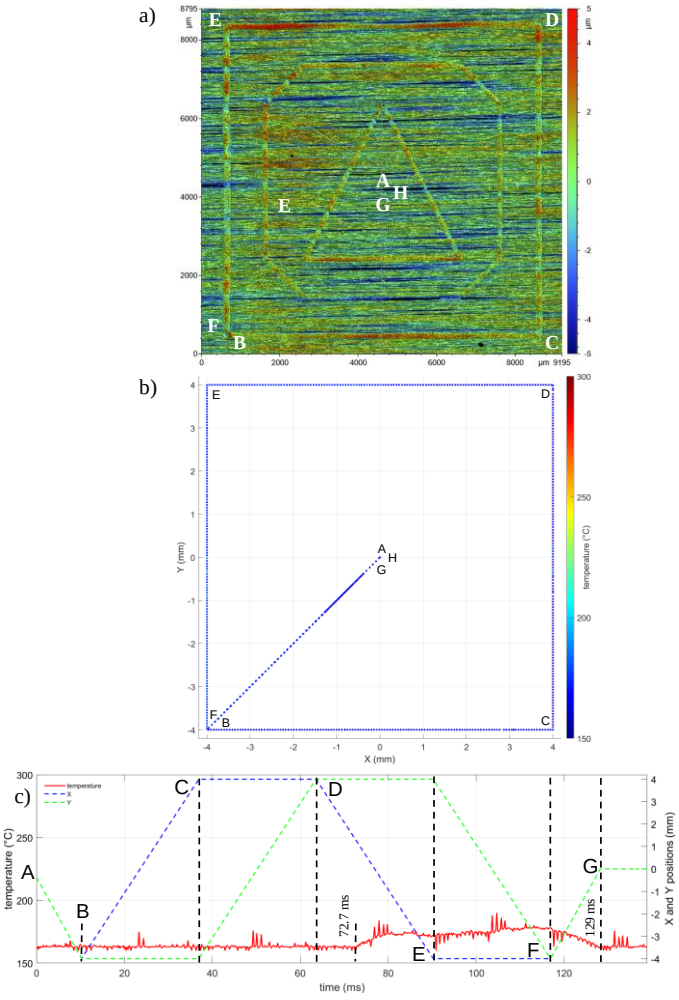

Figure 3. Temperature evolution along the square pattern travelled at 300 mm/s: a) surface topography, b) spatial domain, and c) time domain.

Fig. 4a shows the surface topography associated with the octagon pattern generated through SPa-LRM at 100 mm/s. For a detailed analysis of the temperature evolution, the surface pattern was associated with temperature evolution in spatial and time domains (Fig. 4b and Fig. 4c). Upon visual inspection, the following qualitative and quantitative comments can be made:

- Laser trajectory starts with {0, 0} X_s/Y_s coordinates at point A where laser power is 0 W. Therefore, the pyrometer shows a temperature of 163°C at this point.
- The laser beam makes a first move from center point A to point B along line A-B (null power as well). Then, laser power changes to 30 W at point B and LPa-LRM process begins (Fig. 4a). However, pyrometer does not react instantly.
- This behaviour remains in place the 105 ms timestamp, immediately after making a diagonal turn after point E.

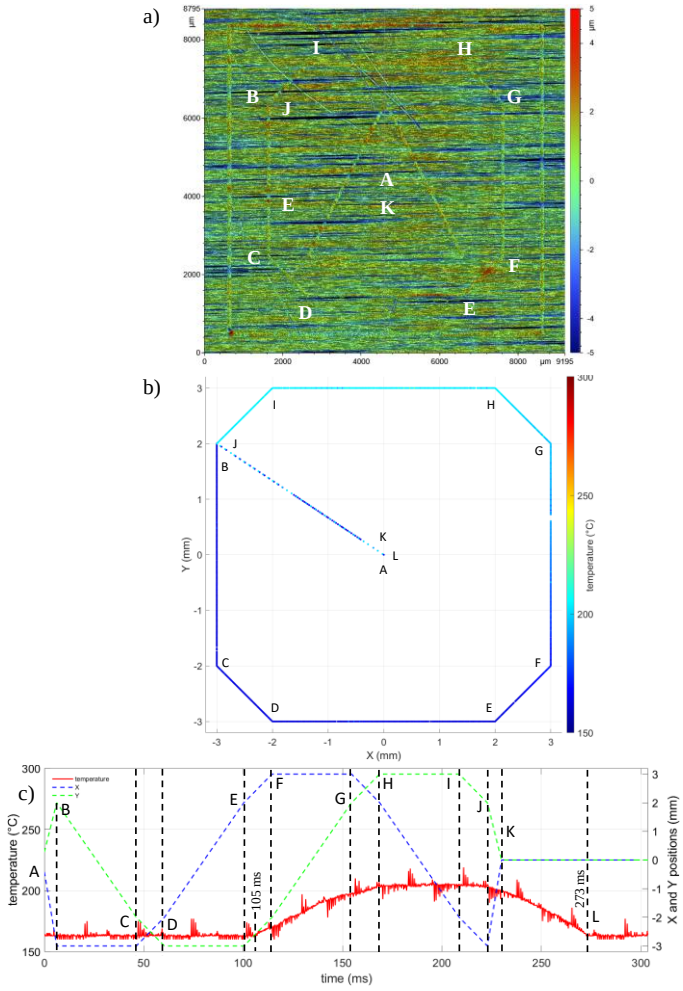

Figure 4. Temperature evolution along the octagon pattern travelled at 100 mm/s: a) surface topography, b) spatial domain, and c) time domain.

- During the next vertical F-G and diagonal G-H moves, temperature reaches its maximum of approximately 203°C at 182 ms timestamp and stays steady along the horizontal H-I and diagonal I-J moves.
- Laser power is reduced to 0 W at point J and laser beam moves back to the center of the octagon with declining temperature.
- Finally, the temperature decreases to 163°C after setting 0 W at 273 ms timestep. This corresponds to the 50 ms time interval.

Similarly to the square pattern scenario, the same octagon pattern was traced at 300 mms and then compared with the 100 mm/s one. Fig. 5a shows the surface topography associated with the octagon pattern generated through SPa-LRM at 300 mm/s. To thoroughly analyze the temperature evolution, the surface pattern was correlated with temperature records in the spatial and time domains (Fig. 5b and Fig. 5c). The main observation from this analysis is the pyrometer was unable to make any temperature readings. Since the scanning speed was 3 time faster the heat dissipation was too slow to overcome/balance the energy delivered along the pattern. Nonetheless, even if the temperature reached was insufficient for pyrometer readings, a sufficient amount of laser energy was delivered for LPa-LRM processing and pattern formation.

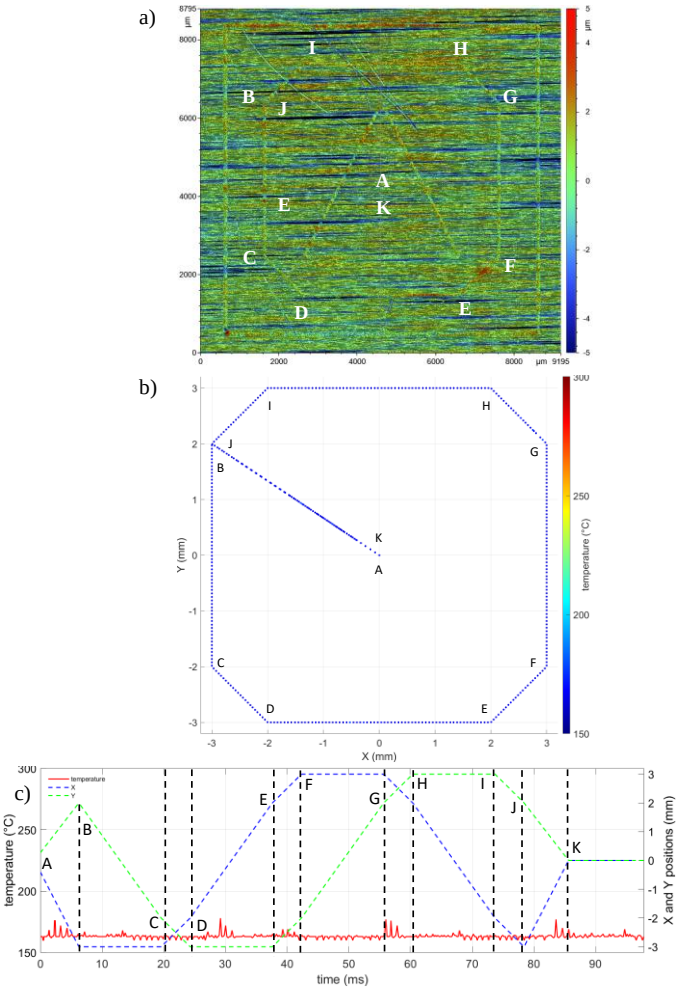

Figure 5. Temperature evolution along the octagon pattern travelled at 300 mm/s: a) surface topography, b) spatial domain, and c) time domain.

The results obtained from the SPa-LRM trials yielded few interesting findings to be detailed further. For the square pattern travelled at 100 mm/s, the temperature started rose above the measurement threshold between point B and C at 38.6 ms timestamp (Fig. 2c). By contrast, when the square trajectory was travelled at 300 mm/s, the temperature became measurable between points D and E at 72.7 ms timestamp (Fig. 3c).

For octagon patterning at 300 mm/s, the temperature never rose above the pyrometer threshold (Fig. 5c), thus suggesting that the overall temperature within an area of 0.9 mm diameter around the molten pool was not preheated enough through heat conduction. In this case, laser energy was solely concentrated on the laser-material interaction zone and was still capable to remelt the material. The entire LPa-LRM process needed about 85 ms to trace the octagon pattern whereas 116 ms were needed when travelling at 100 mm/s. In this later case, the temperature became measurable between points E and F at 105 ms timestamp (Fig. 4c). Of note, the spikes in the overall temperature evolution plots are the result of the electrical noise yielded by the measurement controller of the pyrometer.

As suggested by the experiments detailed above some of the factors that affect the evolution of the temperature during patterning are process speed, trajectory length, and laser power. All these factors are either directly or indirectly related to the balance between the energy delivered and energy dissipated during the process. Because of this, the LRM process will be stable and consistent along the laser path trajectory only when these two components of the balance will be equal. One interesting observation made was that the lower the scanning speed, the earlier is the occurrence of the preheating-by-conduction (PBC) phenomenon that also lasts longer and changes process stability and consistency. However, at higher speeds, PBC effects occurred either later or never depending on the distance travelled along the pattern. When comparing the square and octagon for each speed, longer travel lengths led to more prominent PBC effects. The square pattern – that has longer length than its octagon counterpart – reached a higher maximum temperature for both scanning speeds. Furthermore, unlike the octagon case, the PBC effect was also present when the square pattern was travelled at the higher speed. The maximum temperature attained for the square trajectory at 100 mm/s and 300 mm/s was 253°C and 179°C, respectively, whereas for the octagon the maximums reached 203°C and 163°C, respectively.

IV. Summary and Conclusions

This preliminary study investigates the experimental analysis of temperature distribution evolution in square and octagonal patterns produced by means of the LRM process at two different scanning speeds. Temperature measurements were conducted by means of a two-color pyrometer synchronized with spatial scanning motions. The initial results suggest that temperature distribution evolution is primarily influenced by common process parameters such as scanning speed, trajectory length, pattern configuration, and laser power. The key conclusions drawn from the results:

- The SPa-LRM experiment showed that the scanning speed, travel length, geometry of trajectory, and laser power are parameters that critically influence the local temperature accumulation and pre-heating effects;
- Lower scanning speeds resulted in earlier and longer preheating-by-conduction, whereas higher speeds lead to delayed or inexistent/undetectable preheating-by-conduction effects. The presence/absence of PBC is also critically dependent on the length of the trajectory;
- Based on the observations of the temperature evolution during the LRM of square and octagon patterns with slow and fast speeds, it can be inferred that shorter travel lengths lead to less effective PBC effects and lower temperatures (than in case of longer ones).

The findings presented open up new research directions towards the development of AI-based control and optimization strategies. Future studies are expected to focus on the analysis of temperature evolution during LRM of patterns with sharp corners where the preheating-by-conduction effect should be more evident. The next steps will include thermographic monitoring of the LRM process as a stepping stone towards the development of its digital twin-based cyber-physical system for industrial applications.

Acknowledgment

The work presented in this study is the result of the collaboration between Western University (London, Ontario, Canada) and National Research Council of Canada (London, Ontario, Canada).

References

[1] F. Moglia, J. Pozo, and A.F. Lasagni, “Lasers and surface functionalization,” PhotonicsViews, 2020, 2, pp. 20-22.

[2] F. Esteve, D. Olivier, Q. Hu, and M. Baumers: “Micro-manufacturing technologies and their applications,” I. Fassi and D. Shipley, Eds., Springer International Publishing, Switzerland, 2017, pp. 67-95.

[3] F.D. Ince and T. Özel, “Laser surface texturing of materials for surface functionalization: A holistic review,” Surface and Coatings Technology, 2025, 498, paper 131818, 26 pp.

[4] E. Willenborg, “Polishing with laser radiation,” R. Poprawe, Ed., Tailored Light 2: Laser Application Technology, Springer, 2011, pp. 196-202.

[5] A. Temmler, E. Willenborg, and K. Wissenbach, “Laser Polishing,” Proceedings of SPIE, 2012, 8243, paper 82430W, 13 pp.

[6] E.V. Bordatchev, A.M.K. Hafiz, and O.R. Tutunea-Fatan, “Performance of laser polishing in finishing of metallic surfaces,” The International Journal of Advanced Manufacturing Technology, 2014, 73, pp. 35-52.

[7] A. Temmler, E. Willenborg, and K. Wissenbach, "Design surfaces by laser remelting," Physics Procedia, 2011, 12, pp. 419-430.

[8] F.E. Pfefferkorn and J.D. Morrow, “Controlling surface topography using pulsed laser micro structuring,” CIRP Annals, 2017, 66, pp. 241-44.

[9] E.V. Bordatchev, M. Küpper, S.J. Cvijanovic, E. Willenborg, N. Milliken, A. Temmler, and O.R. Tutunea-Fatan, “Edge-lit sine-shape wedged light guides: Design, optical simulation, laser-remelting-based precision fabrication, and optical performance evaluation,” Precision Engineering, 2020, 66, pp. 333-46.

[10] O. Oreshkin, M. Küpper, A. Temmler, and E. Willenborg, “Active reduction of waviness through processing with modulated laser power,” Journal of Laser Applications, 2015, 27, paper 022004, 7 pp.

[11] T. D. Bennett, D. J. Krajnovich, and L. Li, "Thermophysical modeling of bump formation during CO_2 laser texturing of silicate glasses," Journal of Applied Physics, 1999, 85(1), pp. 153-159.

[12] W. Wang, P. Zou, J. Xu, A. Wang, and X. Wang. “Study on bulge structure formation mechanisms of laser remelting in air atmosphere,” Int’l J of Thermal Sciences, 2024, 206, paper 109348, 24 pp.

[13] Fidan, Sinan, Satılmış Ürgün, Ş Hakan Atapek, Gülşah Aktaş Çelik, Timur Canel, Tamer Sınmazçelik, and Mustafa Özgür Bora. 2025. 'Investigation of surface structuring and oxidation performance of Inconel 718 superalloy by laser remelting with different patterns', Engineering Failure Analysis, 167.

[14] T. Shen and B. Li, “Digital twins in additive manufacturing: a state-of-the-art review,” The Int’l J of Adv Manuf Tech, 2024, 131, pp 63-92.

[15] T. Ozel, “A review on in-situ process sensing and monitoring systems for fusion-based additive manufacturing', Int. J. Mechatronics and Manufacturing Systems, 2023, 16, pp. 115-54.

[16] C.K.P. Vallabh, H. Zhang, D.S. Anderson, A.C. To, and X. Zhao, “Melt pool width measurement in a multi-track, multi-layer laser powder bed fusion print using single-camera two-wavelength imaging pyrometry,” The Int’l J of Adv Manuf Tech, 2024, 132, pp. 2575-2585.

[17] E.V. Bordatchev, S. Cvijanovic, H. Wu, A. Gorski, D. Beyfuss, and R. Tutunea-Fatan, “Conceptualization and preliminary development of statistical digital twin and cyber-thermophysical system for advanced analysis, monitoring, and control of the laser remelting process,” Proc of 2023 IEEE Int’l Conf on Systems, Man, and Cybernetics, pp. 3033-3039.